*Manuscript
Click here to view linked References
https://doi.org/10.1016/j.nanoen.2016.09.032
This is the Pre-Published Version.

Wind Energy and Blue Energy Harvesting Based on Magnetic-Assisted Noncontact Triboelectric Nanogenerator

Long-biao Huang [a]‡, *Wei Xu* [a]‡,*Gongxun Bai* [a,b], *Man-Chung Wong* [a,b], *Zhibin Yang* [a,b], *Jianhua Hao* [a,b,]*

Dr. L.-B. Huang, W. Xu, Dr. G. X. Bai, M.-C. Wong, Z. B. Yang, Prof. J. H. Hao,

[a] Department of Applied Physics, The Hong Kong Polytechnic University, Hong Kong, P. R. China

E-mail: jh.hao@polyu.edu.hk

[b] The Hong Kong Polytechnic University Shenzhen Research Institute, Shenzhen 518057, P. R. China

Highlights:

- We develop magnetic-assisted noncontact triboelectric nanogenerators by utilization of novel polymer composite consisted of magnetic alloy.
- Magnetic-assisted noncontact triboelectric nanogenerator can be used to harvest wind and blue energy
- After encapsulation, the devices show stable performance under high humility environment.

© 2016. This manuscript version is made available under the CC-BY-NC-ND 4.0 license http://creativecommons.org/licenses/by-nc-nd/4.0/.

Abstract

Triboelectric nanogenerator (TENG) as a promising approach has attracted extensive attentions from academic and industry. Herein, a novel strategy of wind and blue energy harvesting based on magnetic-assisted noncontact TENG has been demonstrated. Through the combination of magnetic responsive composite with TENG device, the wind and water forces could be converted into the contact-separation action between Al/Ni electrode and PDMS film. The influence of the relevant parameters (contact-separation frequency, wind speed and humidity, etc.) on the performances of the fabricated TENG has been systematically investigated. The results show the robust potential of magnetic-assisted noncontact TENG for wind and blue energy harvesting applications.

Keywords: triboelectric effect and piezoelectronics, nanogenerator, wind energy, blue energy, non-contact, magnetic-assisted

1. Introduction

Energy harvesting from solar, wind, water wave and ambient mechanical energy has drawn extensive attentions due to the increased carbon emission from limited fossil fuel in the past decades.[1-5] Solar energy and wind energy as zero carbon emission renewables have been developing, aiming at additional supplements to fossil fuel.[6] However, harvesting and conversion of the blue energy, such as tidal energy, wave

energy, thermal energy conversion and osmosis have been under-exploited due to their low power conversion efficiency and relative high cost in engineering.[7]

Recently, triboelectric nanogenerator (TENG) has been used to harvest the wind energy and blue energy.[8-14] Comparing with other green energy harvesting technologies,[2-4, 15, 16] triboelectric nanogenerator, relying on contact electrification and electrostatic induction, has shown remarkable features, including low-cost，diversity in working modes, high-energy conversion efficiency, simply processes for large-scale fabrication and extensive availability of target resource.[17-19] Therefore, TENG has become an attractive device for energy harvesting and a potentially alternative energy source for portable electronics.[11, 17] Furthermore, Wang's group had demonstrated great achievements in wind energy harvesting, such as lawn structured TENG utilized on rooftops with output current density of 0.12 Am^{-2} and power density of 2.76 Wm^{-2}.[8] As aforementioned, blue energy also shows great potential capability as solutions of energy crisis.[12, 14] Correspondingly, triboelectric-electromagnetic hybrid nanogenerator had been developed to harvest broad frequency band blue energy.[14] For the outdoor energy harvesting processes and other applications of TENGs in open environment, those environmental factors, such as gas components, especially humidity have a great influence on the performance of TENG [8, 20, 21]. For example, when the humility increases from 10% to 90%, the open-circuit voltage decreases by about 43%[20, 21]. Therefore, how to avoid the TENG device from those environmental factors becomes one of crucial issues for practical applications. Besides, another important factor affecting the performance of TENG is

the material abrasions between polymer materials/metal electrodes and external force/device materials in conventional operation modes, which may create pollutants, leading to the problems of surface contamination of patterned polymer materials and electrodes, degradation of device materials and the performance decrement of the devices.[22-24] Comparing with in-plane sliding, free-standing[25, 26] and single-electrode types,[27] vertical contact-separation type[28] shows less friction between active layers and electrodes.[23] Recently, the noncontact TENG based on vertical contact-separation mode has been reported to avoid the abrasion of contact materials, showing a promise for energy harvesting.[29, 30] By integrating noncontact TENG with high encapsulation function, the novel design would further provide an opportunity for energy harvesting in harsh environment, such as high humility circumstance.[31]

In order to suit for wind energy and blue energy harvesting in high humility environment, we present a magnetic-assisted noncontact TENG where the device's contact is separated with external mechanical motion. After encapsulation, the TENG device combining the magnetic response layer with TENG active layer is separated from the high humility environment, making the performance of TENG stable. We have systematically investigated various parameters, including contact-separation frequency, wind speed and humility. The results show that the novel magnetic-assisted noncontact TENG can robustly harvest the energy from wind and water flow.

2. Experimental

2.1 Fabrication of triboelectric nanogenerator: To improve the performance of magnetic-assisted noncontact TENG, the conductive Ni fabric was chosen due to its 3D macrostructure, and the 400 nm thick Al film was thermally evaporated on the surface of Ni fabric under the vacuum of 10^{-7} Torr. Then, the as-prepared Al/Ni conductive fabric as an electrode was attached on the surface of arched PET film to serve as one of triboelectric layers. PDMS film was homogeneously formulated by mixing PDMS elastomer and cross-linker with 10:1 weight ratio. After degassing in vacuum oven for 30 min and stored in an oven at 80 ^{o}C for 60 min, the PDMS film with 1.5 μm microwires was peeled from a DVD disc and cut into an appropriate dimension (4 cm × 4 cm) for further device fabrication. The magnetic response layer was fabricated by following the method introduced in our previous report, where magnetic Fe-Co-Ni powder (~ 100 μm, Ciny electric instrument, Ltd) was mixed with PDMS by using 5:1 weight ratio.[30] After degassing in vacuum oven, the composite was cured in an oven at 80 ^{o}C for 60 min and finally cut into suitable dimensions for the subsequent measurements.

2.2 Measurement of electrical performance: LeCroy Wave Runner Oscilloscope (44MXI) with the probe resistance value of 10 MΩ and SR570 low noise current amplifier (Stanford Research System) were used to measure the open-circuit voltage and short-circuit current of TENG, respectively. A commercial linear motor controlled by a computer was used to perform the periodical contact and separation between PDMS film and Al/Ni fabric for the single TENG. Wind speed was measured by

anemometer 8918 (AZ Instrument). A home-made set-up with four TENGs was used for characterizing the performances of wind and water wave energy harvesting.

3. Results and Discussion

The device structure is schematically shown in Figure 1, which includes two parts, magnetic response layer (PDMS/FeCoNi composite/PET/Al/PDMS) and non-magnetic response layer (Al/Ni fabric/PET). To improve the performance of magnetic-assisted noncontact TENG, the Ni fabric was introduced into the non-magnetic response layer due to its excellent mechanical property and 3D structure as shown in SEM image of Figure 1f. The diameter of Ni fiber is around 14 μm consisted of 50 nm sized nanoparticle on the surface as shown in Figure 1f. The Al/Ni fabric serves as electrode and contact surface. The magnetic response layer consists of PDMS/FeCoNi composite and PET/Al/PDMS film. PDMS/FeCoNi composite could be absorbed by a magnet driven by an external force (e.g., wind or water flow) and hence leads to contact-separation between PDMS film and Al/Ni fabric. The arched PET film provides the mechanical supporting and separation between PDMS layer and Al/Ni fabric. The microwires on the surface of PDMS film were replicated from a DVD disc. The working principle of TENG is illustrated in Figure 1b-1e. Under wind and water wave driven, the PDMS film periodically performs contact and separation with Al/Ni fabric. Assuming that the electrical potential of Al/Ni fabric is zero, the triboelectric effect between PDMS film and Al/Ni fabric will generate the positive charges on the Al/Ni fabric and the corresponding

negative charges on the PDMS surface, due to the difference of triboelectric polarities.[32] By performing the separation of PDMS film and Al/Ni fabric, electrical potential difference between Al electrode and Al/Ni fabric electrode is created, resulting in the instantaneous current attributed to the electron flow from Al/Ni fabric to Al electrode as shown in Figure 1e. Therefore, periodically contact and separation between PDMS film and Al/Ni fabric of magnetic-assisted noncontact TENG generates AC signals and therefore converts the mechanical energy into electrical energy. When setting the electric potential of Al/Ni fabric as zero, the electric potential of the PDMS film (U_{PDMS}) can be expressed by

$$U_{PDMS} = \frac{\delta d\prime}{\varepsilon_0} \quad (1)$$

where δ and ε_0 are triboelectric charge density and vacuum permittivity, respectively. And the d' is the gap distance between magnetic-response and nonmagnetic-response layers.[19] The open-circuit voltage reaches its maximum value when PDMS recovers to the original position and is fully separated with Al/Ni fabric. The induced charge density (δ') between PDMS and Al/Ni can be expressed by

$$\delta' = \frac{\delta d\prime \varepsilon_{PDMS}}{\varepsilon_{PDMS} d' + d_{PDMS}} \quad (2)$$

where ε_{PDMS} and d_{PDMS} are relative permittivity of PDMS and thickness of PDMS film, respectively.[33] The parameter δ' depends on the change of the gap distance d', affecting the redistribution of charge between Al electrode and Al/Ni fabric electrode.

A typical electrical output of the as-prepared TENG is shown in Figure 2. Driven

by the liner motor, the patterned PDMS film contacts and separates with Al/Ni fabric periodically in a frequency of 6 Hz with 1 cm distance between device and magnet under the humility of around 30%. The open-circuit voltage (*Voc*) and short-circuit current (*Isc*) were investigated to characterize the performance of device as shown in Figure 2a-2b. The *Voc* and *Isc* can reach up to around 205 *V* and 30 μA, respectively. The electrical output of TENG based on the various resistance of external load is shown in Figure 2c, where *Voc* increases with an increment of external resistance, while *Isc* shows an opposite trend of the variation. The maximum output power of 3.0 mW is achieved at a load resistance of 10 MΩ, which is higher than the reported one in previous literature,[30] possibly thanks to the employment of 3D structure of Al/Ni fabric in this work. Consequently, the as-prepared TENG can lighten 20 white LEDs without external circuit components.

As shown in Figure 3, we further investigated the dependence of open-circuit voltage and short-circuit current of the magnetic-assisted noncontact TENG on the contact-separation frequency between PDMS film and Al/Ni fabric electrode. The results show that the *Voc* and *Isc* are obviously affected by the contact-separation frequency. At elevated low frequency, the change of *Voc* becomes apparent and increases with enhancing frequency. At the frequency of 6 Hz, *Voc* reaches up to the highest value of about 206 V. And then, further increment of contact-separation frequency between magnetic-response layer and non-magnetic-response layer leads to the obvious decrement of *Voc* down to 182 V at 8 Hz and even 175 V at 10 Hz. The *Isc* presents a similar trend as *Voc* in Figure 3b. At low contact-separation frequency,

the *Isc* increases with an increase in the frequency and achieves the maximum value of 30 μA at 6 Hz. Then, *Isc* decreases to around 25 μA at 10 Hz. Under the condition of low frequency, the supporting material of arched PET film has sufficient mechanical strength to allow the magnetic-response layer to leave away from non-magnetic-response layer for fully recovery back to original stage. Accompanying with the increment of frequency, V_{oc} increases from 50 V to 206 V, as an equilibrium is reached when electrons flowing in shorter time.[34] At high frequency, the observation of decrease in *Voc* and *Isc* might be attributed to the following two factors. Firstly, at higher contact-separation frequency, the arched PET film has an insufficient mechanical strength or repulsive force capable of pulling the magnetic-response layer back to form original stage (Figure 1a), which means the gap distance between magnetic responsive and non-magnetic responsive layers might be smaller than the one at original state. Secondly, at the high frequency, the device has no enough time to recover to the original stage due to weak mechanical strength from PET film and the persistent magnetic pull of magnet for fabrics. Accordingly, the gap between magnetic responsive and non-magnetic responsive layers is greatly influenced and decreased. To elucidate the possible mechanism regarding to the effect of gap between PDMS film and Al/Ni fabric electrode on the performance of TENG, COMSOL finite-element program was employed to simulate the electrical potential variation between PDMS film and Al/Ni fabric electrode in this study. As depicted in Figure 4, the calculated electric potential distribution in the device is obviously affected by the magnitude of gap separation between the two layers. As shown in

Figure 4d, the electric potential difference between the Al/Ni fabric electrode and PDMS film for the open-circuit condition decreases when reducing the gap separation. The electric potential difference decreases by about 73.6% from 3.11 kV to 0.82 kV when the gap reduces from 4 cm to 0.5 cm, respectively. The simulation results confirm that the parameter of gap separation between PDMS film and Al/Ni fabric plays an important role in the performance of TENG. Smaller gap between PDMS film and Al/Ni fabric electrode may result in lower electrical potential on the Al/Ni fabric electrode. Particularly, under the condition of the high contact-separation frequency, insufficient mechanical strength and time to recover the original state of arched PET film may reduce the gap between PDMS film and Al/Ni fabric electrode, resulting in lower electric potential on the Al/Ni fabric electrode.

Interestingly, by applying the windsurfing and water baffle to the magnetic-assisted noncontact TENG, the wind and blue energy could be harvested as shown in Figure 5a. The wind or water flow can drive the rotation of whole set-up, which directly leads to the contact-separation of magnetic-assisted noncontact TENGs as shown in Figure 5b. When magnet rotates towards the device, the magnetic response layer could be absorbed, leading to the contact between PDMS film with Al/Ni fabric. In contrast, the separation of PDMS film and Al/Ni fabric is occurred when the magnet rotates away from the device. It should be noted that the novel TENG here is separated with external mechanical motion, which may shorten the lifetime of device and degrade the device materials. With magnetic field mediation, the TENG can be remotely controlled. Moreover, the harvesting of blue energy is also presented in

Figure 5a. The aprons were utilized to block the water flow which drives rotation of the system and results in the contact-separation of TENG. By performing the contact-separation between magnetic response and non-magnetic response layers, the blue energy could be harvested and converted into electrical energy. Apparently, the higher wind speed makes the windsurfing rotating faster, resulting in higher contact-separation frequency between magnetic-assisted and non-magnetic assisted layers. As shown in Figure 5c, the wind speed has a significant effect on the performance of TENG. When increasing wind speed, the contact-separation frequency increases, leading to the higher V_{oc}. However, further increasing the wind speed, the V_{oc} shows an opposing trend. As the above discussion, it is understandable that the observation is attributed to the behavior of supporting material, i.e. arched PET film under different contact-separation frequency.

In practical applications, the TENG inevitably suffers from harsh environment, such as high humility region, which could greatly decrease the performance of TENG. Previous results revealed that the water molecules absorbed on the surface of friction materials could perform discharging effect and reduce the charge creation of TENG. As a solution, an encapsulation of TENG has emerged. Figure 5d shows the open-circuit voltage of un-encapsulated and encapsulated TENG. For un-encapsulated TENG, the *Voc* decreases rapidly when enhancing the relative humility from 10% to 90%. When the relative humility increases from 10% to 70%, the *Voc* decreases from 184 V to 122 V. By further increasing the humility up to 90%, the *Voc* significantly decreases to about 112 V with 64% decline. The results are consistent with the earlier

report by other group.[20] In contrast, the encapsulated magnetic-assisted noncontact TENG shows more stable performance and the *Voc* maintains at around 300 V. Comparing with the great decrease in *Voc* of un-encapsulated TENG, the encapsulated TENG device only shows a slight variation of *Voc* due to measurement deviation. Therefore, the necessity of encapsulation is concluded for practical applications, especially for the energy harvesting under high humility condition. More importantly, by introducing the magnetic response layer into the TENG to form magnetic-assisted noncontact TENG device, the encapsulated TENG is readily separated from external mechanical motion and environments, which could damage electrodes and polymer films. As shown in Figure 5a, when installing four encapsulated magnetic-assisted noncontact TENGs in the system, the wind or blue energy can be harvested and used to lighten 50 white LEDs as illustrated in Figure 5e.

4. Conclusions

In conclusion, a novel wind and blue energy harvesting method based on magnetic-assisted noncontact triboelectric nanogenerator has been demonstrated. Through the combining magnetic responsive layers with TENG device, various types of energy of wind and water forces were converted into a simple motion of typical TENG's working mode, i.e. contact and seperation between Al/Ni electrode and PDMS film. The dependence of relevant parameters (contact-separation frequency, wind speed and humidity, etc.) on the performance of TENG is systematically investigated. The results show the robust potential of magnetic-assisted noncontact

TENG for wind and blue energy harvesting.

Acknowledgements

L.-B.H. and W.X. contributed equally to this work. The research was financially supported by the grants from Research Grants Council of Hong Kong (GRF No. PolyU 5005/13P) and National Natural Science Foundation of China (Grant No. 11474241).

Literature

[1]. Atwater, H. A.; Polman, A., *Nat. Mater.* **2010,** *9* (3), 205-213.
[2]. Stranks, S. D.; Snaith, H. J., *Nat. Nanotechnol.* **2015,** *10* (5), 391-402.
[3]. Green, M. A.; Ho-Baillie, A.; Snaith, H. J., *Nat. Photonics* **2014,** *8* (7), 506-514.
[4]. Shah, A.; Torres, P.; Tscharner, R.; Wyrsch, N.; Keppner, H., *Science* **1999,** *285* (5428), 692-698.
[5]. Hagfeldt, A.; Boschloo, G.; Sun, L.; Kloo, L.; Pettersson, H., *Chem. Rev.* **2010,** *110* (11), 6595-6663.
[6]. Q. Schiermeier , J. T., T. Scully , A. Witze, O. Morton, *nature* **2008,** *454*, 816-823.
[7]. Callawy, E., *nature* **2007,** *450*, 156-159.
[8]. Zhang, L.; Zhang, B.; Chen, J.; Jin, L.; Deng, W.; Tang, J.; Zhang, H.; Pan, H.; Zhu, M.; Yang, W.; Wang, Z. L., *Adv. Mater.* **2016,** *28* (8), 1650-6.
[9]. Meng, X. S.; Zhu, G.; Wang, Z. L., *Acs. Appl. Mater. Inter.* **2014,** *6* (11), 8011-8016.
[10]. Xie, Y. N.; Wang, S. H.; Lin, L.; Jing, Q. S.; Lin, Z. H.; Niu, S. M.; Wu, Z. Y.; Wang, Z. L., *Acs Nano* **2013,** *7* (8), 7119-7125.
[11]. Yang, Y.; Zhu, G.; Zhang, H. L.; Chen, J.; Zhong, X. D.; Lin, Z. H.; Su, Y. J.; Bai, P.; Wen, X. N.; Wang, Z. L., *Acs Nano* **2013,** *7* (10), 9461-9468.
[12]. Chen, J.; Yang, J.; Li, Z. L.; Fan, X.; Zi, Y. L.; Jing, Q. S.; Guo, H. Y.; Wen, Z.; Pradel, K. C.; Niu, S. M.; Wang, Z. L., *Acs Nano* **2015,** *9* (3), 3324-3331.
[13]. Bae, J.; Lee, J.; Kim, S.; Ha, J.; Lee, B. S.; Park, Y.; Choong, C.; Kim, J. B.; Wang, Z. L.; Kim, H. Y.; Park, J. J.; Chung, U. I., *Nat. Commun.* **2014,** *5*. 4929.
[14]. Wen, Z.; Guo, H.; Zi, Y.; Yeh, M.-H.; Wang, X.; Deng, J.; Wang, J.; Li, S.; Hu, C.; Zhu, L.; Wang, Z. L., *Acs Nano* **2016,** *10* (7), 6526-6534.

[15]. Cheng, Y.-J.; Yang, S.-H.; Hsu, C.-S., *Chem. Rev.* **2009,** *109* (11), 5868-5923.
[16]. Hoppe, H.; Sariciftci, N. S., *J. of Mater. Res.* **2004,** *19* (7), 1924-1945.
[17]. Wang, Z. L.; Chen, J.; Lin, L., *Energ. Environ. Sci.* **2015,** *8* (8), 2250-2282.
[18]. Zi, Y.; Wang, J.; Wang, S.; Li, S.; Wen, Z.; Guo, H.; Wang, Z. L., *Nat. Commun.* **2016,** *7*.
[19]. Zi, Y. L.; Niu, S. M.; Wang, J.; Wen, Z.; Tang, W.; Wang, Z. L., *Nat. Commun.* **2015,** *6*.
[20]. Zhang, X. S.; Han, M. D.; Wang, R. X.; Meng, B.; Zhu, F. Y.; Sun, X. M.; Hu, W.; Wang, W.; Li, Z. H.; Zhang, H. X., *Nano Energy* **2014,** *4*, 123-131.
[21]. Nguyen, V.; Yang, R. S., *Nano Energy* **2013,** *2* (5), 604-608.
[22]. Chen, J.; Yang, J.; Guo, H.; Li, Z.; Zheng, L.; Su, Y.; Wen, Z.; Fan, X.; Wang, Z. L., *Acs Nano* **2015,** *9* (12), 12334–12343.
[23]. Li, S. M.; Wang, S. H.; Zi, Y. L.; Wen, Z.; Lin, L.; Zhang, G.; Wang, Z. L., *Acs Nano* **2015,** *9* (7), 7479-7487.
[24]. Han, C. B.; Du, W. M.; Zhang, C.; Tang, W.; Zhang, L. M.; Wang, Z. L., *Nano Energy* **2014,** *6*, 59-65.
[25]. Zhu, G.; Lin, Z. H.; Jing, Q.; Bai, P.; Pan, C.; Yang, Y.; Zhou, Y.; Wang, Z. L., *Nano Lett.* **2013,** *13* (2), 847-853.
[26]. Wang, S. H.; Lin, L.; Xie, Y. N.; Jing, Q. S.; Niu, S. M.; Wang, Z. L., *Nano Lett.* **2013,** *13* (5), 2226-2233.
[27]. Niu, S. M.; Liu, Y.; Wang, S. H.; Lin, L.; Zhou, Y. S.; Hu, Y. F.; Wang, Z. L., *Adv. Funct. Mater.* **2014,** *24* (22), 3332-3340.
[28]. Zhu, G.; Lin, Z. H.; Jing, Q. S.; Bai, P.; Pan, C. F.; Yang, Y.; Zhou, Y. S.; Wang, Z. L., *Nano Lett.* **2013,** *13* (2), 847-853.
[29]. Chen, J.; Yang, J.; Guo, H. Y.; Li, Z. L.; Zheng, L.; Su, Y. J.; Wen, Z.; Fan, X.; Wang, Z. L., *Acs Nano* **2015,** *9* (12), 12334-12343.
[30]. Huang, L. B.; Bai, G. X.; Wong, M. C.; Yang, Z. B.; Xu, W.; Hao, J. H., *Adv. Mater.* **2016,** *28* (14), 2744-2751.
[31]. Guo, H. Y.; Wen, Z.; Zi, Y. L.; Yeh, M. H.; Wang, J.; Zhu, L. P.; Hu, C. G.; Wang, Z. L., *Adv. Energy Mater.* **2016,** *6* (6).
[32]. Wang, Z. L., *Acs Nano* **2013,** *7* (11), 9533-9557.
[33]. Zhu, G.; Pan, C. F.; Guo, W. X.; Chen, C. Y.; Zhou, Y. S.; Yu, R. M.; Wang, Z. L., *Nano Lett.* **2012,** *12* (9), 4960-4965.
[34]. Zhang, X. S.; Han, M. D.; Wang, R. X.; Zhu, F. Y.; Li, Z. H.; Wang, W.; Zhang, H. X., *Nano Lett.* **2013,** *13* (3), 1168-1172.

FIGURE CAPTIONS:

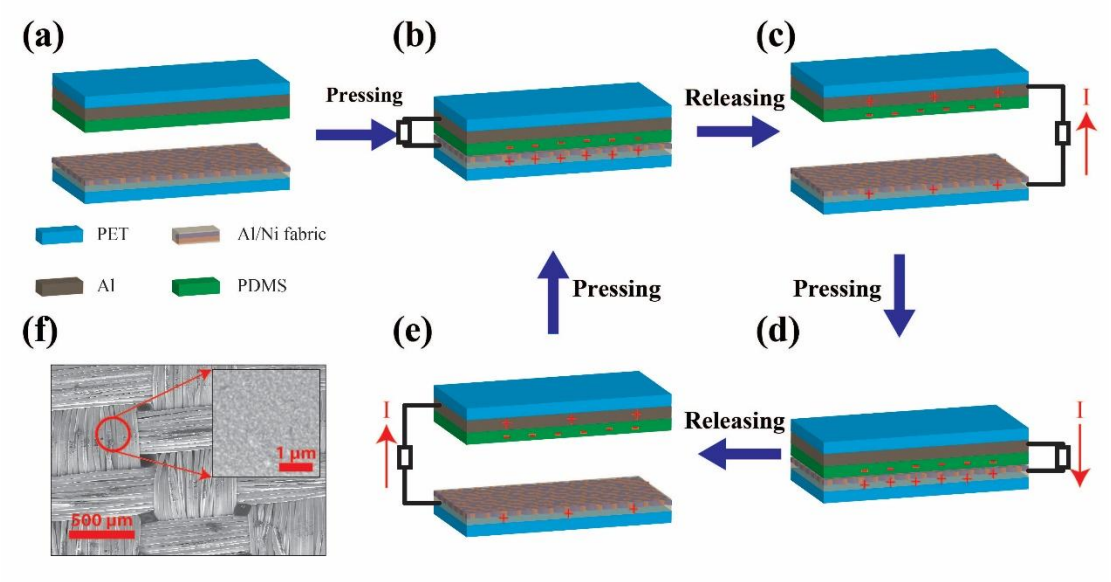

Fig. 1. Structure and fabrication of magnetic-assisted noncontact triboelectric nanogenerator. (a) Schematic illustration of device. (b) - (e) Schematic working principle of device: original state (a); absorption state (b); release state (c); absorption state (d) and release state (e), respectively. (f) SEM images of Ni/Al fabric.

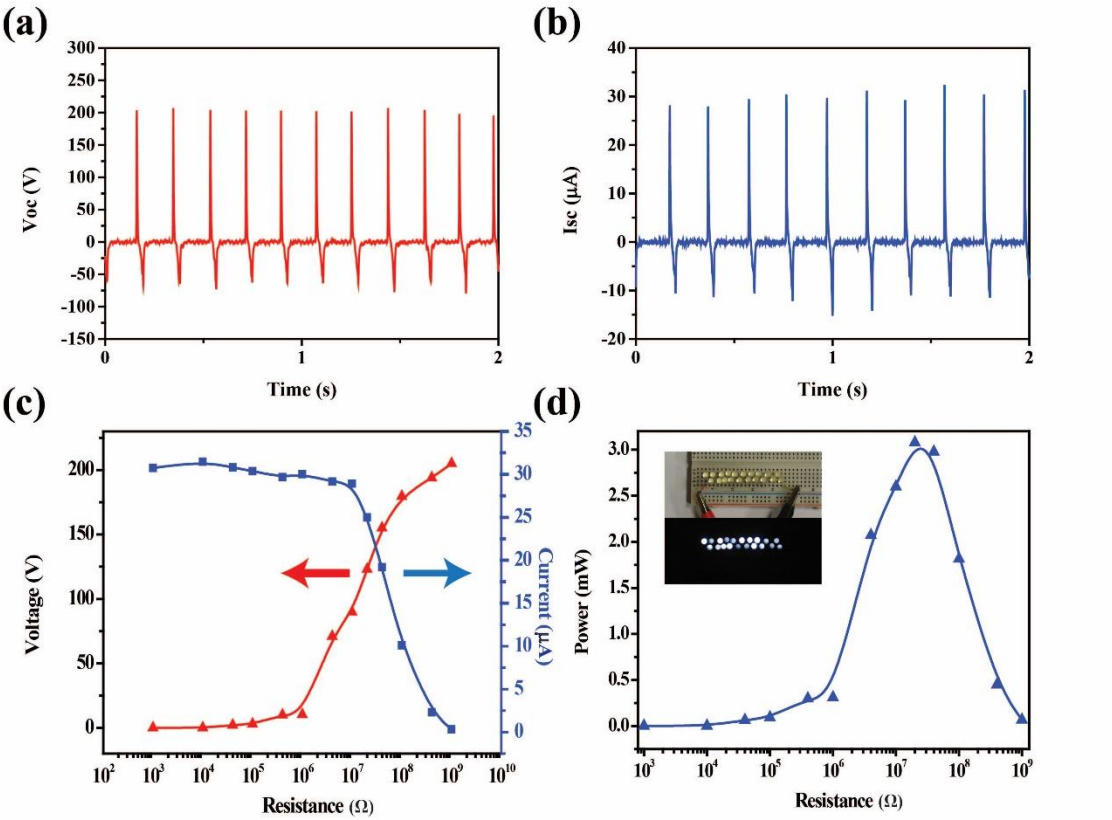

Fig. 2. (a) and (b) Open-circuit voltages and short-circuit current of magnet-assisted noncontact TENG with a frequency of 6 Hz. (c) The dependence of output voltage and current of TENG on the resistance of external load. (d) Dependence of the peak power output on the resistance of external load. Inset photograph shows 20 white LEDs in series without external circuit components.

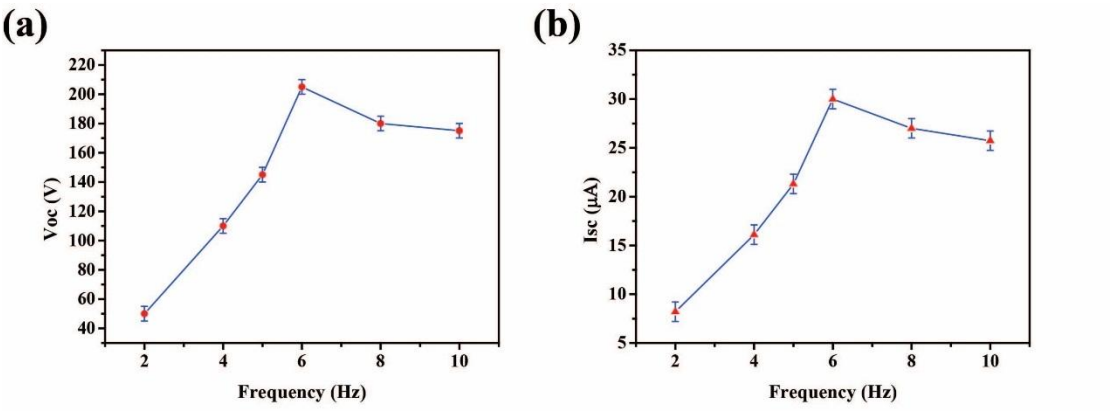

Fig. 3. Dependence of open circuit voltage (a) and short circuit current (b) on the contact-separation frequency.

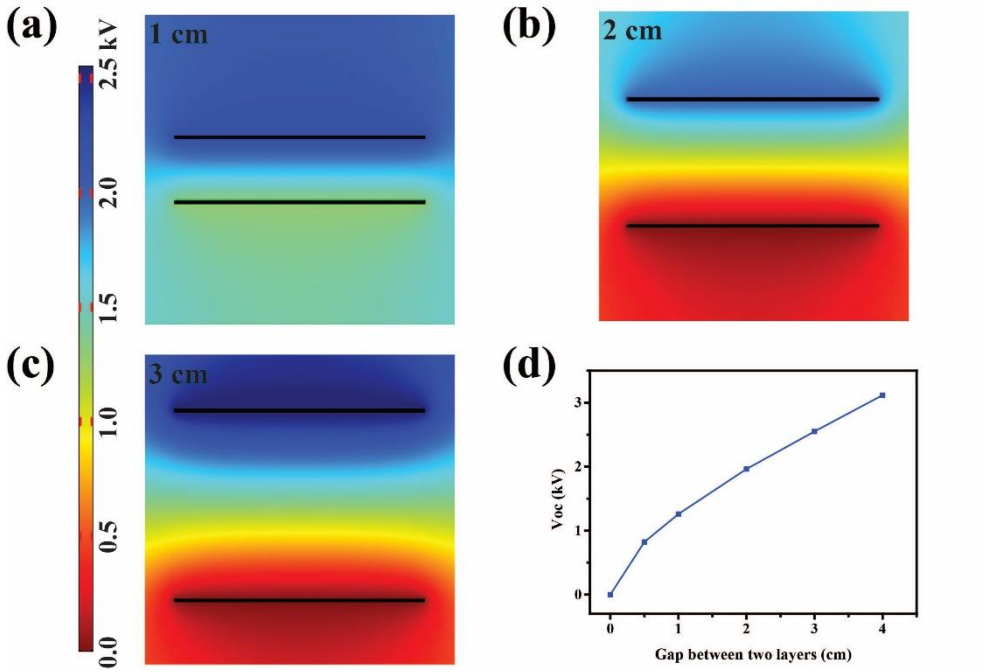

Fig. 4. (a)-(c) Finite-element simulation of the electric potential distribution of device under different gap separation (upper: PDMS film, lower: Al/Ni, triboelectric charge density, -17.5 μC/m^2). (d) Simulated potential of Al/Ni fabric electrode under different gap separation.

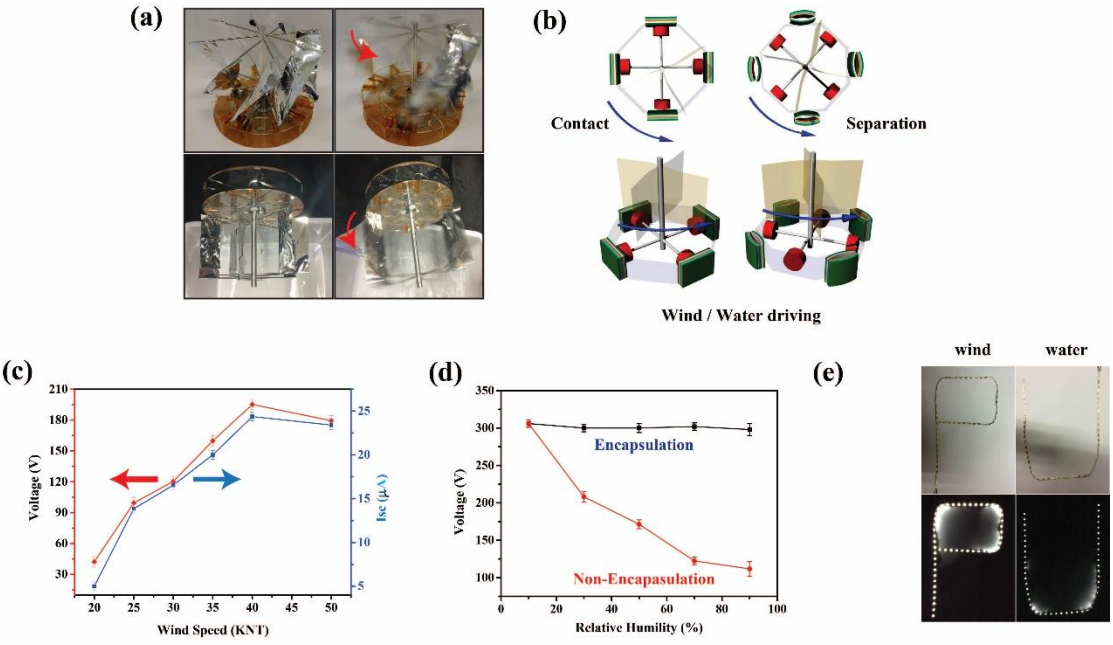

Fig. 5. (a) and (b) Demonstration and schematically illustration of magnetic-assisted noncontact TENG for harvesting energy from wind and water flow (four devices arranged with perpendicular angle). (c) Dependence of open circuit voltage of single TENG on the contact-separation frequency. (d) Performance comparison of single magnetic-assisted noncontact TENG with or without encapsulation. (e) Demonstration of 50 white LED under wind and water driven.

Table of Content